

# How I Do It: Cone-Beam CT during Transarterial Chemoembolization for Liver Cancer<sup>1</sup>

Vania Tacher, MD  
Alessandro Radaelli, PhD  
MingDe Lin, PhD  
Jean-François Geschwind, MD

## Online SA-CME

See [www.rsna.org/education/search/ry](http://www.rsna.org/education/search/ry)

### Learning Objectives:

After reading the article and taking the test, the reader will be able to:

- Discuss the role of cone-beam computed tomography (CBCT) for intraprocedural imaging during transcatheter arterial chemoembolization (TACE)
- Explain the advantages of CBCT over standard 2D angiography in the detection of hepatocellular carcinoma lesions and their feeding arteries
- Describe how CBCT during TACE can be used to assess the technical endpoint of embolization
- Demonstrate how to choose a CBCT technique using a decision-making algorithm to optimize the use of CBCT at each step of TACE for the identification of the lesion, guidance to reach the lesion, and assessment of embolization end points

### Accreditation and Designation Statement

The RSNA is accredited by the Accreditation Council for Continuing Medical Education (ACCME) to provide continuing medical education for physicians. The RSNA designates this journal-based SA-CME activity for a maximum of 1.0 *AMA PRA Category 1 Credit*<sup>™</sup>. Physicians should claim only the credit commensurate with the extent of their participation in the activity.

### Disclosure Statement

The ACCME requires that the RSNA, as an accredited provider of CME, obtain signed disclosure statements from the authors, editors, and reviewers for this activity. For this journal-based CME activity, author disclosures are listed at the end of this article.

<sup>1</sup>From the Russell H. Morgan Department of Radiology and Radiological Science, Division of Vascular and Interventional Radiology, The Johns Hopkins Hospital, 1800 Orleans St, Baltimore, MD 21287 (V.T., J.F.G.); Department of Interventional X-ray, Philips Healthcare, Best, the Netherlands (A.R.); and Department of Clinical Informatics, Interventional, and Translational Solutions, Philips Research North America, Briarcliff Manor, NY (M.L.). Received August 18, 2013; revision requested October 7; revision received November 26; accepted December 3; final version accepted January 20, 2014. Supported by Philips Research North America (Briarcliff Manor, NY) and the French Radiology Society (SFR). Address correspondence to J.F.G. (e-mail: [jfg@jhmi.edu](mailto:jfg@jhmi.edu)).

© RSNA, 2015

Cone-beam computed tomography (CBCT) is an imaging technique that provides computed tomographic (CT) images from a rotational scan acquired with a C-arm equipped with a flat panel detector. Utilizing CBCT images during interventional procedures bridges the gap between the world of diagnostic imaging (typically three-dimensional imaging but performed separately from the procedure) and that of interventional radiology (typically two-dimensional imaging). CBCT is capable of providing more information than standard two-dimensional angiography in localizing and/or visualizing liver tumors (“seeing” the tumor) and targeting tumors through precise microcatheter placement in close proximity to the tumors (“reaching” the tumor). It can also be useful in evaluating treatment success at the time of procedure (“assessing” treatment success). CBCT technology is rapidly evolving along with the development of various contrast material injection protocols and multiphase CBCT techniques. The purpose of this article is to provide a review of the principles of CBCT imaging, including purpose and clinical evidence of the different techniques, and to introduce a decision-making algorithm as a guide for the routine utilization of CBCT during transarterial chemoembolization of liver cancer.

© RSNA, 2015

Online supplemental material is available for this article.

**C**one-beam computed tomography (CBCT) is an imaging technique that acquires three-dimensional (3D) computed tomographic (CT) volumetric images in the angiography suite by using a fixed C-arm system equipped with a flat panel detector (1–4). Since its introduction a decade ago, the utility of CBCT has been demonstrated in multiple disease states including neurovascular disease, peripheral vascular disorders, and oncology (4–10). The step from an exclusive 3D visualization of the vascular structures (rotational angiography—high-contrast imaging) to soft-tissue tomography (CBCT imaging—low-contrast imaging) has opened the door to a range of new applications with low x-ray contrast (4,11). CBCT has improved the feasibility,

effectiveness, and safety of many image-guided procedures thereby allowing physicians to perform procedures that were not possible by using traditional fluoroscopy or digital subtraction angiography (DSA) alone (12–15). CBCT has gained popularity to guide in key procedural steps during transcatheter arterial chemoembolization (TACE) of hepatocellular carcinoma (HCC): tumor detection (“see”), intraprocedural guidance (“reach”), and assessment of treatment success (“assess”). HCC, the most common type of primary liver cancer, is now the second most common cause of cancer death worldwide in a recent 2014 World Health Organization report. TACE is the officially recommended therapeutic option for many patients with HCC according to the Barcelona Clinic Liver Cancer staging and treatment algorithm (16,17). TACE is also the most commonly performed therapy worldwide for patients with HCC. CBCT has been shown to affect diagnosis and treatment in up to 81% of HCC lesions during TACE by providing 3D information that aids in lesion detection, catheter navigation, and assessment of technical success of embolization. These highlights help improve on local progression-free and overall survival (18,19). Numerous CBCT techniques with varying acquisition characteristics and contrast material injection protocols have been described with the goal of seeing, reaching, and assessing treatment success. In addition to exposure settings, CBCT acquisitions may differ by scan acquisition duration, acquisition frame rate, and rotational trajectory. The contrast material injection protocols (rate, volume, concentration, and duration) depend on acquisition settings and the intraarterial catheter/microcatheter location (celiac trunk, superior mesenteric artery, common hepatic artery, proper hepatic artery, selective right or left hepatic artery, and superselective hepatic artery). A summarized overview of CBCT techniques for each specific clinical task (see, reach, assess) is provided in Table 1.

Although the body of evidence has been growing over the last few years

and many physicians and operators recommend its use, there is still no official consensus regarding the use of CBCT during TACE. The aim of this article is to review the general physics and current state of the art for CBCT and to provide an evidence-based rationale for a decision-making algorithm we use to select the most appropriate CBCT technique for each specific clinical task during TACE.

### CBCT Imaging: How It Works

Modern C-arm systems can offer 3D CT x-ray imaging, or CBCT, in addition to conventional two-dimensional (2D) imaging such as fluoroscopy and DSA (7,20). CBCT is enabled by the rotational movement of the C-arm around the patient and requires sophisticated image processing algorithms to calibrate, preprocess, and reconstruct tomographic images with adequate CT-like image quality (21).

### The Principles of Projection Acquisition

CBCT imaging is based on a projection acquisition, whereby the x-ray source and detector are mounted on a C-shaped gantry capable to perform a motorized movement around the patient (Fig 1). During the movement of

### Essentials

- Cone-beam CT (CBCT) provides intraprocedural three-dimensional volumetric imaging during transarterial chemoembolization.
- CBCT techniques have been advanced to improve the visualization and targeting of tumors, and this allows for immediate intraprocedural assessment of transarterial chemoembolization success.
- CBCT is superior to standard two-dimensional angiography in the detection of hepatocellular carcinoma and lesions and their feeding arteries.
- CBCT during transarterial chemoembolization can be used to assess the technical endpoint of embolization, which can then result in a better tumor response and ultimately improved patient survival.
- The choice of CBCT technique to use can follow a decision-making algorithm that optimizes the use of CBCT at each step of transarterial chemoembolization for the identification of the lesion, guidance to reach the lesion, and the assessment of embolization endpoints.

### Published online

10.1148/radiol.14131925 **Content codes:** GI CT

**Radiology 2015;** 274:320–334

### Abbreviations:

CBCT = cone-beam CT  
 CBCT-A = CBCT during arteriography of an extrahepatic branch  
 CBCT-AP = CBCT during arterial portography  
 CBCT-HA = CBCT during hepatic arteriography  
 Deb-CBCT = unenhanced CBCT after DEB-TACE  
 DEB-TACE = TACE with drug-eluting beads  
 DP-CBCT = dual-phase CBCT during hepatic arteriography  
 DSA = digital subtraction angiography  
 HCC = hepatocellular carcinoma  
 Lip-CBCT = unenhanced CBCT after conventional TACE  
 TACE = transcatheter arterial chemoembolization  
 3D = three-dimensional  
 2D = two-dimensional

### Funding:

This research was supported by the National Institutes of Health (grants CA160771 and P30 CA006973).

Conflicts of interest are listed at the end of this article.

**CBCT Techniques to “See,” “Reach,” and “Assess” Treatment Success during TACE**

CBCT Technique	Contrast Medium Injection Protocol				Imaging Protocol				Outcomes/Expected Results
	Volume*	Concentration*	Speed*	Microcatheter/ Catheter Tip Position	No. of CBCT Scans	Scan Duration	Delay*	Tumor Detection and Tumor-feeding Arteries Visualization	
CBCT-HA	12–64 mL	100–370 mg iodine per milliliter	1–12 mL/sec	CHA/PHA/SHA	Single	5–10 seconds	2–10 sec	Tumor and feeding arteries detection	
DP-CBCT	18–60 mL	150–370 mg iodine per milliliter	1.5–2 mL/sec	CHA/PHA/SHA	Dual	5–10 seconds	First scan: 3–15 seconds; second scan: 28–47 seconds	First phase: hypervascular tumor and tumor feeding vessel enhancement; second phase: either tumor parenchymal enhancement (early acquisition) or corona enhancement (delayed acquisition) Tumor detection	
CBCT-AP	30–90 mL	150–370 mg iodine per milliliter	2–4 mL/sec	SMA	Single	5–10 seconds	20–40 seconds	Tumor detection	
CBCT-A	12–24 mL	300 mg iodine per milliliter	4 mL/sec	Extrahepatic artery	Single	5–10 seconds	~4 seconds	Confirmation of tumor vascularization by extrahepatic arterial supply	
Lip-CBCT	...	...	...	...	Single	5–10 seconds	...	Lipiodol deposition	
DP-CBCT	18–60 mL	150–370 mg iodine per milliliter	1.5–2 mL/sec	CHA/PHA/SHA	Dual	5–10 seconds	First scan: 3–15 seconds; second scan: 28–47 seconds	Tumor devascularization	
Deb-CBCT	...	...	...	...	Single	5–10 seconds	...	Tumor contrast medium saturation	

Note.—The delay is the amount of time elapsed after start of the contrast medium injection and before the start of the acquisition. This ensures the vessels are completely filled with contrast medium during imaging. CBCT-A = CBCT during arteriography of an extrahepatic branch; CBCT-AP = CBCT during arterial portography; CBCT-HA = CBCT during hepatic arteriography; CHA/PHA/SHA = common hepatic artery/proper hepatic artery/selective hepatic artery (right or left hepatic artery); Deb-CBCT = unenhanced CBCT after DEB-TACE; DP-CBCT = TACE with drug-eluting beads; DP-CBCT = dual-phase CBCT during hepatic arteriography; Lip-CBCT = unenhanced CBCT after conventional TACE; SMA = superior mesenteric artery.  
\* Data are ranges.

Figure 1

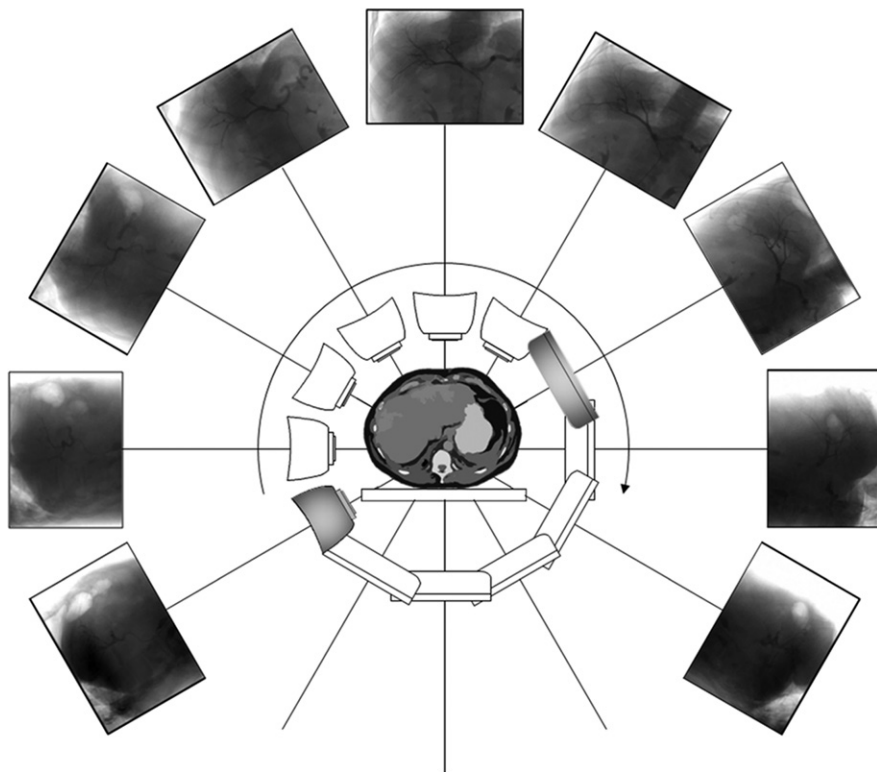


**Figure 1:** CBCT imaging involves the rotation of a C-arm equipped with a flat panel detector around the patient. Multiple 2D projections are acquired and reconstructed to generate a 3D volumetric data set.

the system, x-ray projection images of the object are acquired along multiple angular directions, following a circular path covering an angular range of at least 200°. This is the minimum angular range to fulfill the 180° plus fan-angle criterion for data acquisition (22–24). The target area is positioned in the center of rotation (isocenter) and CBCT volumes are then obtained by integrating information from the 2D high-resolution projection images. In contrast to classic multidetector CT acquisitions, the motion path includes an acceleration and deceleration phase encompassing a phase of constant speed of 30°–60° per second and projection acquisition is performed in pulsed mode. Tube and detector settings depend on the clinical application. For abdominal imaging, typical tube parameters are 5–10-msec pulses per projection at 120-kVp tube voltage including copper filtration with frame

rates of 30–60 frames per second. The use of flat detectors has been key in the development of CBCT imaging due to high resolution, high detector quantum efficiency, high frame rate, high dynamic range, small image lag, and excellent linearity (25). Flat detectors are based on a thin-film cesium iodide scintillator coupled to a charge-coupled device fabricated on a large-area panel (26–32). Recent detectors cover a planar region of 19 × 25 cm and up to 30 × 40 cm for a reconstructed volume of 25 × 25 × 19 cm to 30 × 30 × 40 cm at a high spatial resolution on the order of 150 × 150 μm<sup>2</sup> pixel size (33,34). Projection acquisition includes the use of one-dimensional antiscatter grids to suppress scattered photons.

#### Volumetric Reconstruction

The projections of the rotational scan are transferred directly to the reconstruction computer to produce

volumetric data. The 3D CBCT reconstruction uses a modified Feldkamp filtered back-projection that is a straightforward generalization of the 2D filtered back-projection to cone-beam geometry (25). A complexity for tomographic reconstruction on interventional C-arm systems is the need to accurately measure the true system position, which needs to be taken into account during back projection. This is determined from the geometric calibration. Parker weighting is applied to compensate line integrals measured more than once and a source attenuation correction is applied to correct for nonequiangular sampling during acceleration and deceleration (4,35). Patient dose considerations and general lack of clinical necessity result in practical CBCT spatial resolution of the order of 0.5 × 0.5 × 0.5 mm<sup>3</sup>, which is achieved by adapting the focal, spot size, detector readout resolution, and the reconstruction filter (21).

#### Postprocessing

Data acquired from the rotational acquisition are automatically reconstructed and displayed on the workstation as a 3D rendering and/or in axial, coronal, sagittal, or oblique planes. CBCT images can be postprocessed and manipulated on a separate 3D workstation in the control room. Modern systems also allow for manipulation at table side with a sterile mouse and/or a remotely connected touch screen. Postprocessing software is available for different applications to increase the spatial resolution in a region of interest, to correct for photon starvation or artifacts due to metal objects, or to quantify anatomic information such as vascular length and diameter or the size of a lesion (36).

#### CBCT Radiation Exposure

The x-ray exposure associated with CBCT has been the subject of several studies performed on phantoms, animals, patients, and the medical team (5,37–42). The x-ray exposure may vary between manufacturers depending on parameters such as tube voltage, tube current, filter thickness and material, and number of projections (42–45). The

estimated effective dose to the patient for one CBCT scan of the abdomen is approximately 3–10 mSv, approximately three to four times less than the comparable dose in an abdominal multidetector CT scan (10–12 mSv) (41,43,46). The routine use of CBCT during TACE increases the dose-area product when compared with the use of DSA alone (37). The dose-area product is defined as the radiation dose per square centimeter ( $\text{Gy} \cdot \text{cm}^2$ ) of accumulated skin exposure and represents an estimated measurement of the entire amount of energy delivered to the patient by the x-ray beam, and it can be used as an indicator for the stochastic risk (47). On the other hand, the additional use of CBCT decreases the deterministic risk (cumulative dose) when compared with a procedure using fluoroscopy and DSA alone and facilitates the procedure, potentially reducing the procedure time (37). As for all interventional procedures using x-ray exposure, the operators should wear protective devices and leave the examination room when performing 3D scans, and CBCT acquisition should be used judiciously (37,40).

### Limitations of CBCT

The contrast-to-noise ratio of CBCT images is 1.5 to 2 times lower when compared with that of conventional multidetector CT, primarily due to less-advanced antiscatter radiation technology (42,48). On the other hand, due to finer detector pitch, its spatial resolution is superior. The combination of high spatial resolution and intraarterial administration of iodinated contrast material compensates for the lower contrast resolution and provides a high-quality tumor depiction along with detailed vascular anatomy. As a result, CBCT has been shown to provide diagnostic information during TACE comparable to the level of imaging modalities such as multidetector CT and magnetic resonance (MR) imaging (49–51). Nevertheless, CBCT images are susceptible to artifacts due to noise, scatter, partial volume effects, truncation artifacts, beam hardening, ring artifacts, and motion artifacts. Several algorithms have been developed to reduce noise

and motion artifacts during reconstruction or to modify the x-ray spectrum (2,52–57). Respiratory motion is particularly problematic in CBCT imaging of the liver because any motion leads to strong degradation of the image quality, inducing streaking and blurring, especially when iodinated contrast material is injected. Early CBCT implementations required acquisition times of 10 to 20 seconds; today most commercial fixed C-arm systems can offer acquisition times of less than 10 seconds. CBCT scan protocols that require only 3–8 seconds have shown to minimize breathing artifacts and maximize patient comfort (5,58–60). Another potential limitation of CBCT imaging is its limited field of view when compared with multidetector CT. Methods to perform CBCT with a larger field of view have been developed, although data are limited and the feasibility in clinical practice and effect on clinical workflow has to be considered. The limited field of view of CBCT images may not include the entire liver. However, the effect of this on tumor assessment appears to be minor. As reported by Meyer et al, the maximum transversal liver diameter varies approximately between 15 and 27 cm, thus a field of view of  $25 \times 25 \times 19$  cm is sufficient when the patient is correctly positioned on the angiographic table (61). Appropriate review of preprocedural imaging is important to guide the correct patient positioning and field of view centering to include all targeted tumors.

### Patient and Equipment Setup

#### General Precaution

Patient breath holding is essential in obtaining appropriate image quality. Patients are instructed to hold their breath at end-expiration during each CBCT acquisition. Free breathing is allowed between the early and delayed phase scans in the case of dual-phase CBCT acquisition. We ask the patient to stop breathing 2–3 seconds before starting CBCT acquisition. If necessary, oxygen is administered to patients during the acquisition to minimize

the discomfort of breath holding. The breathing routine should be practiced with the patient prior to imaging and therefore deep conscious sedation should be avoided.

#### Patient Positioning and Equipment Set-up

Under mild sedation, the patient is placed in a supine position on the angiography table. The position of the patient on the angiographic table is such that the C-arm can rotate around the patient in the head position and that the liver is included in the CBCT field of view (Fig 2). In view of the limitations in field of view, the radiologist should consider off-center patient positioning with respect to the table center line especially in patients with tumors at the periphery of the livers, marked hepatomegaly, or in obese patients. A test rotational movement is then performed to ensure that the C-arm can rotate around the patient unobstructed. All C-arm CT systems require similar test runs to avoid collisions during the actual rotational acquisition.

#### Catheterization during TACE

An angiographic catheter (4 or 5 F) is used to sequentially select the superior mesenteric artery and the celiac axis. DSA of the superior mesenteric artery should be performed to assess portal vein patency. Celiac and common or proper hepatic artery angiograms are obtained to delineate hepatic arterial anatomy and blood supply to the tumors, reveal the presence of aberrant arterial anatomy, and identify tumor blush. The 2D imaging runs are acquired by using the same imaging system equipped with CBCT. The CBCT imaging system allows for 3D intraprocedural imaging feedback at each step of TACE. Once the positioning of the microcatheter in the targeted vessels is verified by means of 2D angiography and CBCT, the chemotherapeutic and embolic agents are delivered. Most commonly, the chemotherapeutic agent is either mixed with ethiodized oil (Lipiodol Ultra-fluide; Laboratoire Guerbet, Aulnay-sous-Bois, France) in conventional TACE or loaded into calibrated microspheres in DEB-TACE.

Figure 2



**Figure 2:** Configuration of angiography suite during TACE. The C-arm is aligned with the table and positioned at the head end, and accessory equipment (eg, shielding screens, intravenous poles) is positioned in such way that it can be easily removed to allow for 3D scanning. The large monitor shows patient monitoring information and different imaging inputs, including live fluoroscopy, 2D angiography, and the results of the embolization planning and guidance software overlaid on live fluoroscopy images.

### CBCT to “See” the Tumor: Rationale and Techniques

#### Rationale

Preprocedural diagnostic imaging provides information to plan the intervention, while intraprocedural imaging guides the intervention. Systematically, the images obtained during the procedure are compared with those from preprocedural diagnostic imaging, including contrast-enhanced MR imaging and/or multiphase multidetector CT to confirm that the initial plan matches with the intraprocedural plan. The starting point in interventional oncology is visualization to localize the tumor(s) targeted for therapy. Correct tumor localization increases the selectivity of drug delivery into the targeted tumor(s) and limits nontarget embolization, thereby preserving healthy liver tissue and optimizing tumor response

(62,63). CBCT imaging provides detailed information on tumor vascularity, location, size, and volume. The ability of CBCT to enable visualization of HCC lesions has been evaluated in the literature for its sensitivity in HCC detection when compared with other diagnostic imaging modalities and/or its diagnostic accuracy. The diagnostic accuracy involves an evaluation of the degree of confidence of readers in characterizing a mass in the liver as HCC (64,65). CBCT is superior to DSA in the detection of liver tumors and can achieve a degree of intraprocedural HCC detection comparable to preprocedural diagnostic imaging including contrast-enhanced MR imaging and multiphase multidetector CT (5,23,24,38,59–61,66–71). CBCT can depict typical HCC diagnostic imaging features such as hypervascular tumor enhancement and tumor parenchymal enhancement, on the arterial and parenchymal phases, respectively,

and corona enhancement around the hypervascular core of the HCC on the delayed venous phase (22,23,71,72). Nevertheless, the ability of CBCT in depicting HCC depends on the CBCT technique (detection sensitivity from 86% for CBCT-HA to near 100% for CBCT-AP) and the imaging modality used as reference standard for comparison (multiphase multidetector CT, contrast-enhanced MR imaging, DSA, CT during arterial portography). A summary of the literature on the different CBCT techniques available to use to “see” the tumor intraprocedurally is provided in Table E1 (online).

#### CBCT Techniques

**CBCT-HA.**—CBCT-HA is the most common technique for intraprocedural HCC detection and is recommended as part of the CardioVascular and Interventional Radiological Society of Europe/Society of Interventional Radiology protocol guidelines for selective TACE (9,64,65,71). This technique involves a single CBCT acquisition with one contrast medium injection through a catheter or a microcatheter positioned in the celiac trunk, common hepatic artery, proper hepatic artery, or selective right or left hepatic artery. Depending on the contrast medium injection protocol and especially on the delay of CBCT acquisition after contrast medium injection, CBCT-HA may be used for three purposes: to demonstrate the tumor-feeding arteries, the hypervascular component of the targeted tumor, or the corona enhancement. The contrast medium injection protocol (volume of contrast medium, dilution, injection rate, and the delay of image acquisition) may be adjusted to obtain an optimal liver-to-tumor contrast (73). The use of diluted or full iodinated contrast medium concentration depends on the specific manufacturer’s acquisition settings. Nonetheless, an acquisition delay after injection start of 2–10 seconds, and an injection rate of 1–12 mL/sec of iodinated contrast medium have been favored in most studies, depending on the catheter tip location and the CBCT imaging system manufacturer. CBCT-HA has the ability to depict occult HCC

lesions unseen on nonselective DSA images during TACE and has shown similar diagnostic accuracy and positive predictive value to those of multiphasic multidetector CT (24,64,65).

**CBCT-AP.**—The CBCT-AP technique exploits the fact that in the portal washout phase, HCC is hypoenhancing compared with adjacent healthy liver parenchyma. CBCT-AP is performed by using a single CBCT acquisition after one contrast medium injection (30–90 mL of nondiluted contrast medium [range, 150–370 mg iodine per milliliter] or 1:1 diluted with saline) through a catheter placed in the superior mesenteric artery with an acquisition delay after injection start of 20–40 seconds, at a rate of 2–4 mL/sec. The advantage of using CBCT-AP is the ability to detect the full extent of the tumor burden and evaluate portal vein patency. This technique has been included in a number of other research studies either as an independent tool to detect targeted tumor(s) or in association with other CBCT techniques to add complementary diagnostic information about HCC imaging features and maximize intraprocedural tumor detection accuracy. CBCT-AP provides high detection sensitivity of small HCCs (<30 mm) when compared with CT during arterial portography (65,74,75). CT during arterial portography was described as the most sensitive modality to detect HCC in 1983 before the advent of diagnostic multiphasic multidetector CT and contrast-enhanced MR imaging. Unlike CBCT-HA, CBCT-AP is used only to localize the HCC lesion and to determine its size. Its detection sensitivity can reach 100% compared with preprocedural multiphasic multidetector CT, either alone or in combination with CBCT-HA (70). Likewise to CBCT-HA, CBCT-AP has also the ability to depict occult HCC lesions unseen on nonselective DSA images during TACE (68).

**DP-CBCT.**—DP-CBCT is performed through the acquisition of two consecutive CBCT scans with one contrast medium injection through a catheter or microcatheter positioned in the celiac trunk, common hepatic artery, proper hepatic artery, or selective right or

left hepatic artery. Depending on the catheter/microcatheter tip location, DP-CBCT is achieved after one contrast media injection (18–60 mL of nondiluted contrast medium [range, 150–370 mg iodine per milliliter] or diluted 1:1 with saline), at a rate of 1.5–2 mL/sec. Depending on contrast media injection and CBCT acquisition parameters, DP-CBCT can display the arterial tumor enhancement and tumor feeding arteries on the first scan (arterial phase, 3–15-second acquisition delay), and either the parenchymal tumor enhancement (parenchymal phase, 28-second acquisition delay) or the corona enhancement on the second scan (delayed venous phase, 40–47-second acquisition delay). The advantages of DP-CBCT are that it provides different types of information with a single imaging protocol by displaying two different phases of contrast enhancement. The combination of an arterial and a delayed parenchymal CBCT has been shown to be superior to CBCT-HA alone in depicting HCC nodules and provides a detection sensitivity of 94% when preprocedural contrast-enhanced MR imaging, the gold standard for HCC detection, is used as a reference (66). The parenchymal phase of a DP-CBCT scan is able to better depict the tumor boundaries than the first arterial phase (Figs 3–5, A and B). The ability of the second parenchymal phase CBCT to provide precise delineation of tumor boundaries has also been validated using a semi-automatic volumetric segmentation technique comparing CBCT, diagnostic volumetric imaging (contrast-enhanced MR imaging or multiphasic multidetector CT) and pathology samples in preclinical and clinical settings (60,76). A longer delay time (40–47 seconds) between the two phases allows for better depiction of the corona enhancement, which helps to distinguish HCC from arteriportal shunt (71). DP-CBCT has also been combined with CBCT-AP to achieve a diagnostic sequence depicting HCC features normally observed with multiphasic multidetector CT imaging. This combination has shown high detection sensitivity (100%) and the ability to even depict HCC lesions undetected

at preprocedural multiphasic multidetector CT (59,71).

### CBCT to “Reach” the Tumor: Rationale and Techniques

#### Rationale

Determination of the patient’s hepatic vascular anatomy and tumor arterial supply are critical to completely treat the tumors with the chemoembolic material and to avoid nontarget embolization (77–79). The availability of CBCT volumetric information can be used to achieve comprehensive visualization of hepatic arterial anatomy and tumor feeding arteries and determine the degree of selectivity of drug delivery to the targeted tumor(s), thus reducing the risk of nontarget embolization and potential complications. Volumetric CBCT datasets are acquired in a calibrated coordinate space and are synchronized with the C-arm, flat detector, and angiographic table movements. This can be exploited during the intervention to facilitate the selection of the best viewing angle to reach the tumor(s) and to guide catheter navigation by using fluoroscopy overlay on the 3D dataset (59). Several studies have explored the value of CBCT and automated software in improving the detection accuracy of tumor-feeding vessels and the feasibility of displaying 3D hepatic arterial tree and tumor-feeding arteries acquired from CBCT overlaid on top of live fluoroscopy (19,38,58,59,67,69,77,80,81). The additional value of CBCT in detecting extrahepatic feeding arteries has also been investigated (78,82–84). A summary of the studies and CBCT techniques used to “reach” HCC tumors is provided in Table E2 (online).

#### CBCT Techniques

**CBCT-HA.**—CBCT-HA can be used in the same acquisition to “see” and to “reach” HCC lesions since it provides hepatic arterial anatomy and the early arterial enhancement of the targeted tumor(s). A comparison of CBCT-HA with preprocedural imaging is recommended because it may alert to the need to search for additional feeding

Figure 3

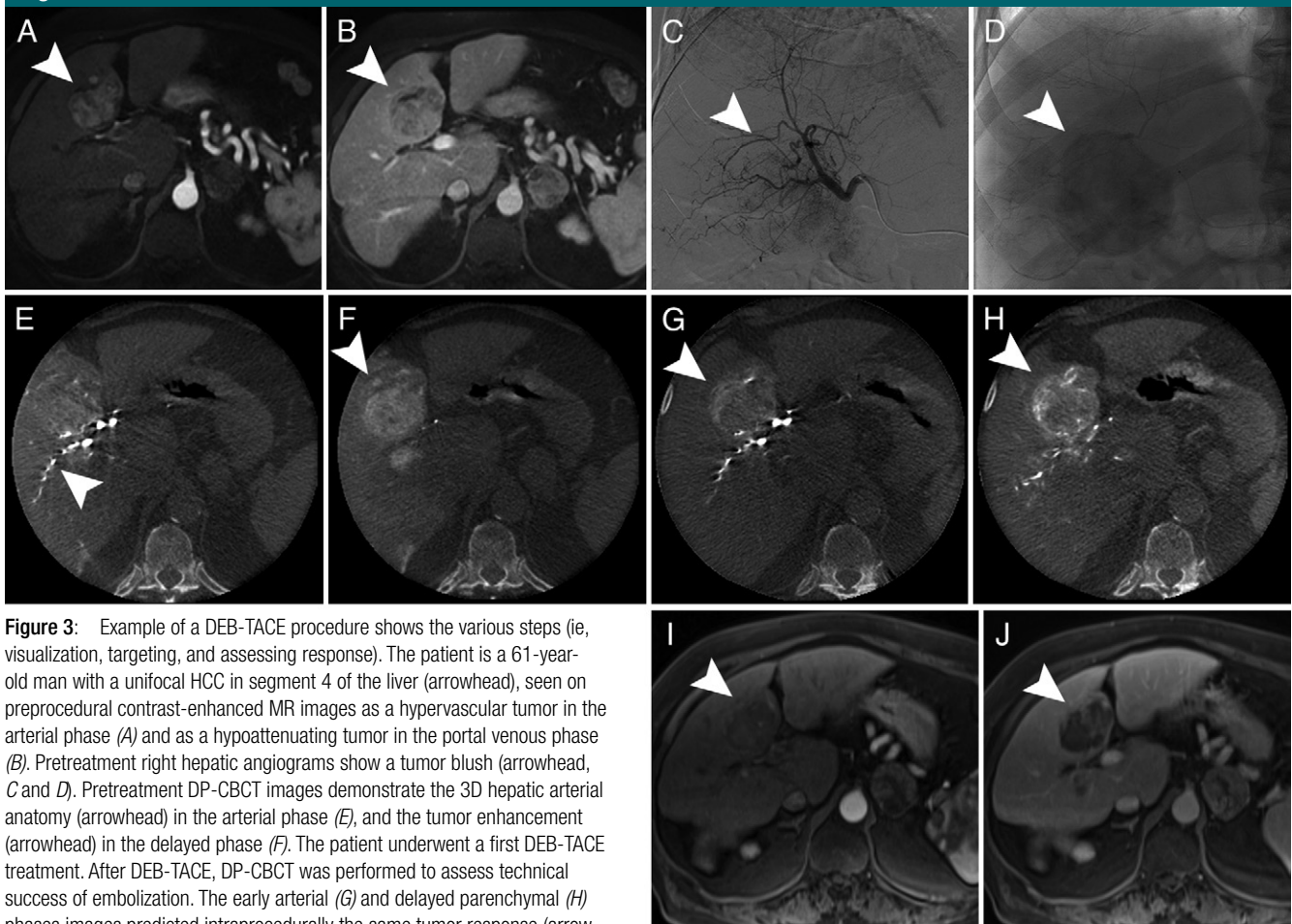


**Figure 3:** Example of a DEB-TACE procedure shows the various steps (ie, visualization, targeting, and assessing response). The patient is a 61-year-old man with a unifocal HCC in segment 4 of the liver (arrowhead), seen on preprocedural contrast-enhanced MR images as a hypervascular tumor in the arterial phase (A) and as a hypoattenuating tumor in the portal venous phase (B). Pretreatment right hepatic angiograms show a tumor blush (arrowhead, C and D). Pretreatment DP-CBCT images demonstrate the 3D hepatic arterial anatomy (arrowhead) in the arterial phase (E), and the tumor enhancement (arrowhead) in the delayed phase (F). The patient underwent a first DEB-TACE treatment. After DEB-TACE, DP-CBCT was performed to assess technical success of embolization. The early arterial (G) and delayed parenchymal (H) phases images predicted intraprocedurally the same tumor response (arrowhead) when compared with the post-TACE follow-up contrast-enhanced MR images obtained 1 month later in the arterial (I) and portal venous (J) phases.

arteries or extrahepatic arterial supply. The sensitivity and specificity of CBCT-HA in the detection of the tumor-feeding artery are superior to those of non-selective DSA (97% vs 77% and 97% vs 73%, respectively) when lipiodol deposition into the tumor at 1-week unenhanced multidetector CT follow-up is used as the reference standard (58,59,85). However, identification of tumor feeders on CBCT datasets can be tedious and time consuming, especially when multiple feeders and multiple lesions have to be targeted.

**DP-CBCT.**—The first and second phase scans can be used not only for tumor detection but also to facilitate identification of the tumor-feeding arteries. The first CBCT scan provides the

early arterial enhancement of the liver allowing 3D visualization of the hepatic arterial anatomy and of the hypervascular tumor core, while the second CBCT scan provides delayed parenchymal phase imaging of the liver, which offers a more precise delineation of the tumor boundaries, thus facilitating the identification of the tumor feeding arteries (38,80).

**CBCT-A.**—CBCT has the ability to show incomplete tumor enhancement, which may be indicative of extrahepatic supply. To perform TACE effectively, superselective catheterization is essential not only through hepatic branches but also through extrahepatic collaterals. The extrahepatic tumor arterial supply may involve up to 28% of patients

undergoing TACE for HCC (82). The most commonly identified extrahepatic feeders include the right inferior phrenic artery, omental arteries, adrenal artery, and intercostal and subcostal arteries (82). CBCT-A involves the injection of contrast medium through a microcatheter positioned into suspected extrahepatic tumor feeding arteries. The CBCT-A technique has clearly demonstrated the ability to provide vascular anatomy details of the left and right inferior phrenic and the intercostal artery and to be superior to 2D angiography alone in ensuring technical success (82–84). An acquisition delay of 4 seconds and an injection rate of 3–4 mL/sec of nondiluted iodinated contrast medium were favored in most studies (78,82–84).

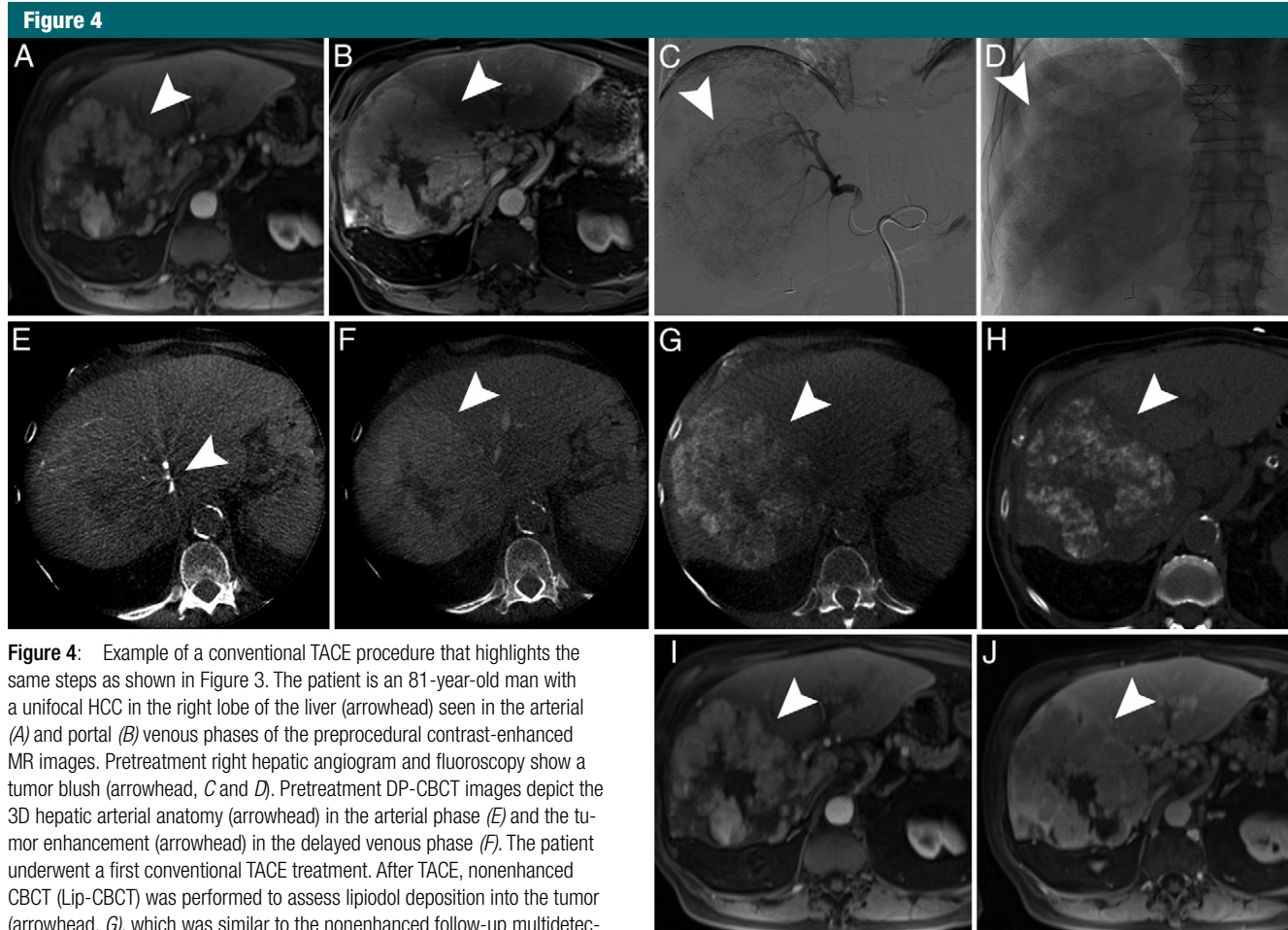


**Figure 4:** Example of a conventional TACE procedure that highlights the same steps as shown in Figure 3. The patient is an 81-year-old man with a unifocal HCC in the right lobe of the liver (arrowhead) seen in the arterial (A) and portal (B) venous phases of the preprocedural contrast-enhanced MR images. Pretreatment right hepatic angiogram and fluoroscopy show a tumor blush (arrowhead, C and D). Pretreatment DP-CBCT images depict the 3D hepatic arterial anatomy (arrowhead) in the arterial phase (E) and the tumor enhancement (arrowhead) in the delayed venous phase (F). The patient underwent a first conventional TACE treatment. After TACE, nonenhanced CBCT (Lip-CBCT) was performed to assess lipiodol deposition into the tumor (arrowhead, G), which was similar to the nonenhanced follow-up multidetector CT study (H). The incomplete lipiodol uptake (arrowhead) was predictive of poor tumor response on the 1-month follow-up contrast-enhanced MR images in both the arterial (I) and portal venous (J) phases.

*Three-dimensional embolization planning and guidance software.*—Two technologies (Flight Plan for Liver, GE Healthcare, Chalfont St Gilles, England or EmboGuide, Philips Healthcare, Best, the Netherlands) capable to intraprocedurally assist in the detection of the tumor feeding arteries and guide microcatheter positioning in 3D have been recently described (58,59,85). Although technical differences exist, the basic workflow involves the identification of the targeted lesions on the CBCT dataset and the automatic extraction of candidate feeders to the targets. The use of the delayed parenchymal CBCT scan of a DP-CBCT for tumor boundary delineation is preferred unless a better visualization is achieved on the arterial

phase or a CBCT-AP scan (38,59,80). Interactive 3D segmentation provides a precise tumor boundary delineation with minimal user interaction and time effort (60,76). After automatic feeding artery extraction, this and the segmented targeted tumor(s) can then be manipulated and displayed together with a 3D visualization of the CBCT dataset using a volume rendering technique. After verification, the 3D plan and the (segmented) targeted tumor(s) are overlaid on live fluoroscopy to create a 3D roadmap (Fig 5, E). Automatic software for tumor feeding artery detection on 3D volumetric CBCT images has been shown to be equivalent or superior to manual detection on CBCT or nonselective DSA images,

while improving the clinical workflow (58,59,65).

The 3D roadmap follows the rotation and angulation movements of the C-arm and translations of the table and automatically adjusts to magnification changes. The operator can move the C-arm into a position that best facilitates catheterization, minimizes vessel overlap and foreshortening, without losing the matching between live fluoroscopy and the angiographic roadmap. The 3D roadmap can be manually adjusted in case of patient movement, thus further mitigating the need for creating a new roadmap and minimizing the use of iodinated contrast medium and x-ray exposure when compared with 2D angiography alone (58,59,85). The use of

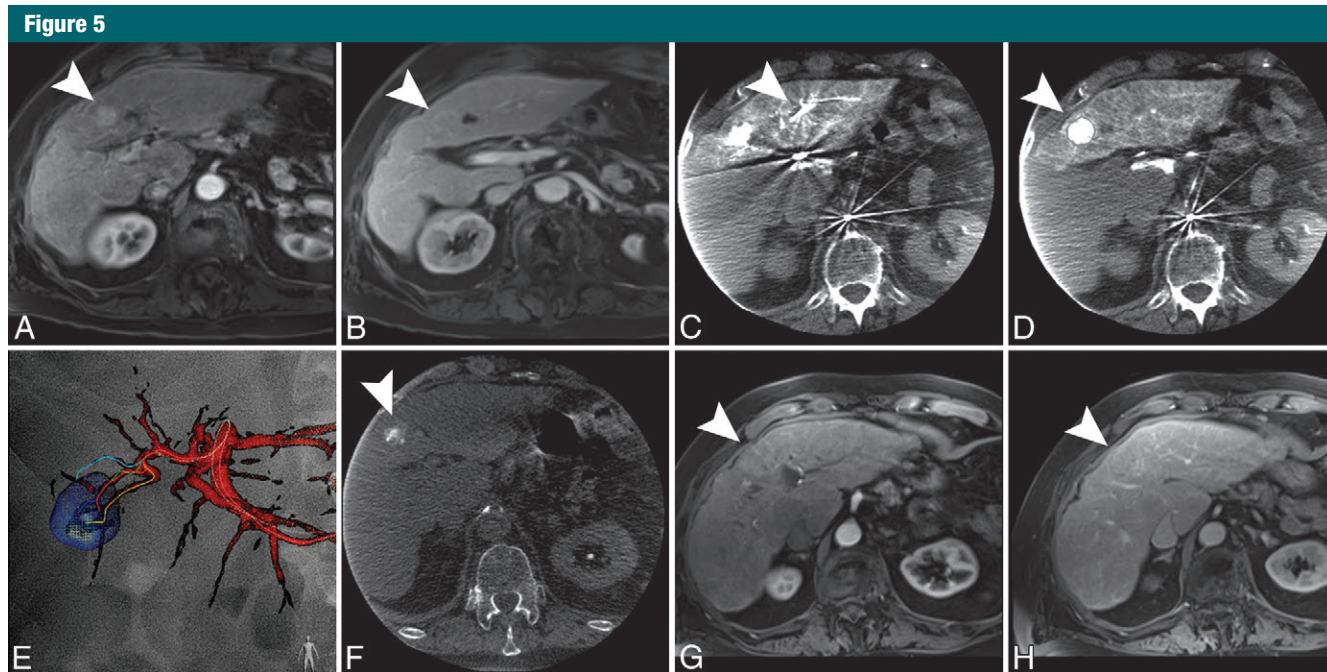


**Figure 5:** Example of a superselective DEB-TACE procedure performed using software guidance technology. The patient is a 79-year-old man with a unifocal HCC in segment 4 of the liver (arrowheads), seen in the arterial (A) and portal venous (B) phases of the preprocedural contrast-enhanced MR images. Pre-TACE DP-CBCT images demonstrate the 3D hepatic arterial anatomy (arrowhead) in the arterial phase (C) and the tumor enhancement (arrowhead) in the delayed venous phase (D). Software allowed tumor segmentation and 3D roadmap generation to reach the targeted tumor (E). The patient subsequently underwent successful DEB-TACE therapy. After DEB-TACE, nonenhanced CBCT (Deb-CBCT) was performed to assess contrast medium saturation at the tumor margin (arrowhead, F). The degree of contrast medium saturation at the tumor margin predicted tumor response on the 1-month follow-up contrast-enhanced MR images in both the arterial (G) and portal venous (H) phases.

the 3D roadmapping has been shown to be feasible and precise (58,59).

Automatic computed analysis software is able to achieve greater than 90% sensitivity in tumor feeding artery detection of hypervascular HCC lesions, 7%–20% higher than visual identification on CBCT-HA datasets by an experienced operator and 29%–50% higher than visual identification on a nonselective DSA study (58,59,85). Automated software may also be used to detect the cystic artery and select the optimal microcatheter position for drug delivery to avoid non-target embolization (78).

#### CBCT to “Assess” Treatment Success: Rationale and Techniques

##### Rationale

Assessing treatment success during TACE is critically important as it affects

treatment endpoints and consequently tumor response, local progression-free, and overall survival (18,59).

The objective of posttreatment CBCT is to provide immediate assessment of tumor coverage and offer the possibility to change catheter positioning to ensure complete treatment of tumor burden and even predict tumor response (39,86–90). Incomplete tumor treatment negatively impacts survival (91,92). The imaging characteristics of different chemoembolic agents differ substantially, thus requiring different post-treatment CBCT techniques. Lipiodol is a radiopaque contrast agent, which has also been used as a biomarker for HCC (93). Lipiodol deposition in the tumor is a prognostic factor affecting local recurrence of HCC and may be determined directly during the procedure using unenhanced CBCT, which offers equivalent lipiodol detection

accuracy to unenhanced MDCT imaging (91,92,94–96). Drug-eluting beads, commonly loaded with doxorubicin (adriamycin), are radiolucent and so are mixed with contrast agent during delivery. These beads occlude tumor-feeding arteries from where the chemotherapy diffuses locally into the tumor (97,98). Assessment of DEB-TACE therefore requires the visualization of tumor-feeding vessel devascularization or tumor contrast agent saturation features on CBCT images (39,99). The value of immediate post-procedural CBCT scanning has been explored in several studies, which are detailed in Table E3 (online).

##### CBCT Techniques

**Lip-CBCT.**—Lip-CBCT is a technique used to assess the lipiodol deposition into the tumor after drug delivery (Fig 4, G). This technique involves the acquisition of a CBCT scan without

Figure 6

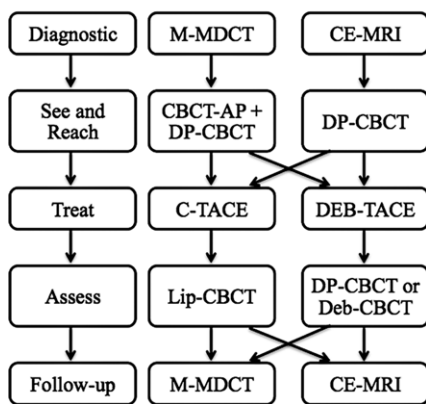


**Figure 6:** A suggested algorithm for the optimal use of different CBCT techniques during each successive step of diagnostic, intraprocedural (“see”, “reach” the targeted tumors, and “assess” treatment success), and follow-up imaging. For example, a patient with multiphasic multidetector (M-MDCT) diagnostic imaging would benefit from intraprocedural CBCT-AP plus DP-CBCT to “see” and “reach” the tumor, or a patient with contrast-enhanced MR imaging (CE-MRI) would benefit from DP-CBCT. According to treatment type, conventional TACE (C-TACE) or DEB-TACE, Lip-CBCT would help to assess intraprocedural treatment success after conventional TACE just as DP-CBCT or Deb-CBCT after DEB-TACE. Finally, follow-up diagnostic imaging based on multiphasic multidetector CT or contrast-enhanced MR imaging would be performed at 4–6 weeks after treatment.

contrast medium injection immediately after conventional TACE treatment. Incomplete deposition of lipiodol into the tumor may be indicative of extrahepatic supply or incomplete delivery (90). Lip-CBCT imaging provides immediate feedback to the operator with lipiodol conspicuity equivalent to unenhanced multidetector CT and is predictive of tumor response when compared with 1-month follow-up multiphasic multidetector CT or contrast-enhanced MR imaging (68,90,95,96). The use of Lip-CBCT helps to achieve complete iodized oil filling of tumor(s) and therefore improves therapeutic effects by optimizing the embolization endpoint (90). Intraprocedural Lip-CBCT depicts HCC with 100% sensitivity compared with preprocedural diagnostic imaging (59,68,91,94).

**Deb-CBCT.**—Deb-CBCT is a technique that involves a single non-contrast-enhanced CBCT scan after DEB-TACE to assess treatment success by visually estimating the degree of marginal contrast material saturation of the entire tumor volume, which is used as a surrogate for the beads deposition location and can help in determining the embolization endpoint (Fig 5F). With Deb-CBCT, the positive predictive value of tumor response for a marginal contrast agent saturation above 75% on Deb-CBCT images is 85% (99).

**DP-CBCT.**—The aim of DP-CBCT after DEB-TACE is to assess treatment success by displaying the changes in contrast enhancement of the target tumor(s) on both phases owing to tumor feeding vessel devascularization (Fig 3G, H). The same protocol of the DP-CBCT technique as described above is used also after treatment, ensuring that the same microcatheter positioning and contrast agent injection protocols are used. DP-CBCT helps to assess the lack of contrast agent uptake in the tumor whereas Deb-CBCT depicts the contrast agent uptake of the tumor margins, in both cases indicating successful tumor coverage with DEB-TACE. DP-CBCT has also shown to be predictive of tumor response according to the European Association for Study of the Liver and the Response Evaluation Criteria in Solid Tumors guidelines at 1-month follow-up contrast-enhanced MR imaging (39). Limited tumor enhancement changes on DP-CBCT images after DEB-TACE may suggest to the operator either the need for retreatment or to search for additional feeding arteries. Commonly, the post-DEB-TACE DP-CBCT technique displays an arterial tumor enhancement and tumor-feeding arteries on the first scan (arterial phase, 3–15-second acquisition delay), and then parenchymal tumor enhancement on the second (parenchymal phase, 28-second acquisition delay).

#### Suggested Algorithm for the Optimal Use of the Various CBCT Techniques during Each TACE Step

The optimal and systematic use of the various CBCT techniques during each

TACE step has been summarized in a suggested algorithm (Fig 6). Two CBCT techniques may be recommended for tumor localization: DP-CBCT in case of preprocedural contrast-enhanced MR imaging (detection sensitivity: 94%–100%) or CBCT-AP plus DP-CBCT (detection sensitivity: 100%) in case of preprocedural multiphasic multidetector CT. The benefits of CBCT-AP in addition to DP-CBCT is to ensure high HCC detection, especially for HCC lesions not detected on preprocedural multiphasic multidetector CT images. The first phase of the DP-CBCT can be used to define hepatic arterial anatomy and tumor feeding arteries. The second, late arterial phase of the DP-CBCT may be used to more accurately identify the boundaries of the targeted tumor. Automated software facilitates the identification of tumor-feeding arteries and provides a 3D roadmap throughout fluoroscopic device manipulation, with a potential reduction in iodinated contrast medium administration and x-ray exposure. To assess treatment success after chemoembolic agent delivery, the choice of the CBCT technique depends on the type of treatment: Lip-CBCT after conventional TACE or either Deb-CBCT or DP-CBCT after DEB-TACE.

#### Conclusion

CBCT is becoming an essential tool in interventional oncology. CBCT provides 3D volumetric information that is critical for the main procedural steps in intraarterial liver therapy for HCC: tumor localization (“see”), planning and guidance for catheterization (“reach”), and intraprocedural evaluation of treatment success (“assess”). We have reviewed technical details and clinical evidence for all the existing CBCT techniques, with the aim of generating an algorithm to guide the selection of the most appropriate CBCT technique for each procedural step (Fig 6 [with three illustrative clinical examples, Figs 3–5]). Two CBCT techniques provide the highest diagnostic accuracy for tumor localization: DP-CBCT alone or in combination with CBCT-AP. The first phase of the DP-CBCT study depicts

the hepatic arterial anatomy and early tumor enhancement. The second or parenchymal phase accurately identifies the boundaries of the targeted tumor and/or shows late enhancing lesions undetected in the arterial phase. The addition of CBCT-AP may facilitate HCC detection and referencing to preprocedural multiphase multidetector CT by capturing the portal venous hypoenhancement, which is typical of HCC. CBCT-HA or the first phase of a DP-CBCT examination can be used to map the hepatic anatomy and determine the tumor-feeding branches. CBCT is superior to standard 2D angiography in depicting tumor-feeding branches either through visual inspection or in combination with automated feeding detection software. Automated software provides the highest detection accuracy of tumor-feeding arteries with a faster workflow and offers a 3D roadmap throughout fluoroscopic device manipulation, with a potential reduction in iodinated contrast material administration and x-ray exposure. The choice of CBCT technique to assess treatment success after chemoembolic agent delivery depends on the type of treatment. Lip-CBCT is used after conventional TACE and has near equivalent capabilities to determine lipiodol distribution and defects as postprocedural multidetector CT. Deb-CBCT or DP-CBCT is used after DEB-TACE. Deb-CBCT depicts the intratumoral distribution and defects of the iodinated contrast material mixed with the drug-eluting beads during therapy delivery. Contrast material saturation in tumor margins on Deb-CBCT images has a high predictive value of short-term tumor response. This technique should be used in the case of subsegmental therapy delivery. DP-CBCT follows instead the rationale of postprocedural multiphase MR imaging or multidetector CT and illustrates the decrease in tumor enhancement due to therapy. Significant reduction in tumor enhancement between DP-CBCT scans acquired before and after TACE is a predictor of short-term tumor response. The utilization of CBCT during TACE of HCC has shown to be valuable beyond technical success

and short-term tumor response. The utilization of CBCT is an independent factor associated with lower local recurrence rates at 3-year follow-up and longer overall survival.

In summary, in light of the substantial clinical evidence available in the literature, we recommend that CBCT should be accepted as standard of care for imaging in intraarterial therapy of HCC.

**Disclosures of Conflicts of Interest:** V.T. disclosed no relevant relationships. A.R. disclosed no relevant relationships. M.L. disclosed no relevant relationships. J.F.G. Activities related to the present article: grant from Philips Medical. Activities not related to the present article: consultant (personal fees) to Nordion, Biocompatibles/BTG, and Bayer Healthcare; grants from DOB, Biocompatibles/BTG, Bayer Healthcare, Nordion, Context Vision, Guerbet. Other relationships: disclosed no relevant relationships.

## References

1. Feldkamp LA, Davis LC, Kress JW. Practical cone-beam algorithm. *J Opt Soc Am A* 1984;1(6):612-619.
2. Grass M, Guillemaud R, Rasche V. Interventional x-ray volume tomography. In: Grangeat P, ed. *Tomography*. London, England: ISTE/Wiley, 2009; 287-306.
3. Saint-Felix DM, Picard CL, Ponchut C, Romeas R, Rougee A, Troussset YL. Three dimensional x-ray angiography: first in-vivo results with a new system. In: Kim Y, ed. *Proceedings of SPIE: medical imaging 1993—image capture, formatting, and display*. Vol 1897. Bellingham, Wash: SPIE—The International Society for Optical Engineering, 1993; 90-98.
4. Grass M, Koppe R, Klotz E, et al. Three-dimensional reconstruction of high contrast objects using C-arm image intensifier projection data. *Comput Med Imaging Graph* 1999;23(6):311-321.
5. Hirota S, Nakao N, Yamamoto S, et al. Cone-beam CT with flat-panel-detector digital angiography system: early experience in abdominal interventional procedures. *Cardiovasc Intervent Radiol* 2006;29(6):1034-1038.
6. Mistretta CA, Grist TM. X-ray digital subtraction angiography to magnetic resonance-digital subtraction angiography using three-dimensional TRICKS. Historical perspective and computer simulations: a review. *Invest Radiol* 1998;33(9):496-505.
7. Racadio JM, Babic D, Homan R, et al. Live 3D guidance in the interventional radiology suite. *AJR Am J Roentgenol* 2007;189(6):W357-W364.
8. Richter G, Engelhorn T, Struffert T, et al. Flat panel detector angiographic CT for stent-assisted coil embolization of broad-based cerebral aneurysms. *AJNR Am J Neuroradiol* 2007;28(10):1902-1908.
9. Wallace MJ, Kuo MD, Glaiberman C, et al. Three-dimensional C-arm cone-beam CT: applications in the interventional suite. *J Vasc Interv Radiol* 2009;20(7 Suppl):S523-S537.
10. Wiesent K, Barth K, Navab N, et al. Enhanced 3-D-reconstruction algorithm for C-arm systems suitable for interventional procedures. *IEEE Trans Med Imaging* 2000;19(5):391-403.
11. Söderman M, Babic D, Holmin S, Andersson T. Brain imaging with a flat detector C-arm: Technique and clinical interest of XperCT. *Neuroradiology* 2008;50(10):863-868.
12. Tacher V, Lin M, Desgranges P, et al. Image guidance for endovascular repair of complex aortic aneurysms: comparison of two-dimensional and three-dimensional angiography and image fusion. *J Vasc Interv Radiol* 2013;24(11):1698-1706.
13. Abi-Jaoudeh N, Kruecker J, Kadoury S, et al. Multimodality image fusion-guided procedures: technique, accuracy, and applications. *Cardiovasc Intervent Radiol* 2012;35(5):986-998.
14. Kobeiter H, Nahum J, Becquemin JP. Zero-contrast thoracic endovascular aortic repair using image fusion. *Circulation* 2011;124(11):e280-e282.
15. Lin CJ, Blanc R, Clarençon F, et al. Overlying fluoroscopy and preacquired CT angiography for road-mapping in cerebral angiography. *AJNR Am J Neuroradiol* 2010;31(3):494-495.
16. Kwan SW, Kerlan RK Jr, Sunshine JH. Utilization of interventional oncology treatments in the United States. *J Vasc Interv Radiol* 2010;21(7):1054-1060.
17. Llovet JM, Burroughs A, Bruix J. Hepatocellular carcinoma. *Lancet* 2003;362(9399):1907-1917.
18. Iwazawa J, Ohue S, Hashimoto N, Muramoto O, Mitani T. Survival after C-arm CT-assisted chemoembolization of unresectable hepatocellular carcinoma. *Eur J Radiol* 2012;81(12):3985-3992.
19. Kakeda S, Korogi Y, Ohnari N, et al. Usefulness of cone-beam volume CT with flat panel detectors in conjunction with catheter angiography for transcatheter arterial embolization. *J Vasc Interv Radiol* 2007;18(12):1508-1516.
20. Mistretta CA, Crummy AB, Strother CM. Digital angiography: a perspective. *Radiology* 1981;139(2):273-276.

21. Orth RC, Wallace MJ, Kuo MD; Technology Assessment Committee of the Society of Interventional Radiology. C-arm cone-beam CT: general principles and technical considerations for use in interventional radiology. *J Vasc Interv Radiol* 2008;19(6):814–820.
22. Matsui O, Kadoya M, Kameyama T, et al. Benign and malignant nodules in cirrhotic livers: distinction based on blood supply. *Radiology* 1991;178(2):493–497.
23. Ueda K, Matsui O, Kawamori Y, et al. Hypervascular hepatocellular carcinoma: evaluation of hemodynamics with dynamic CT during hepatic arteriography. *Radiology* 1998;206(1):161–166.
24. Willatt JM, Hussain HK, Adusumilli S, Marrero JA. MR Imaging of hepatocellular carcinoma in the cirrhotic liver: challenges and controversies. *Radiology* 2008;247(2):311–330.
25. Ning R, Chen B, Yu R, Conover D, Tang X, Ning Y. Flat panel detector-based cone-beam volume CT angiography imaging: system evaluation. *IEEE Trans Med Imaging* 2000;19(9):949–963.
26. Antonuk LE, Boudry J, Huang W, et al. Demonstration of megavoltage and diagnostic x-ray imaging with hydrogenated amorphous silicon arrays. *Med Phys* 1992;19(6):1455–1466.
27. Antonuk LE, Jee KW, El-Mohri Y, et al. Strategies to improve the signal and noise performance of active matrix, flat-panel imagers for diagnostic x-ray applications. *Med Phys* 2000;27(2):289–306.
28. Antonuk LE, Yorkston J, Huang W, Siewerdsen J, Street RA. Considerations for high frame rate operation of two-dimensional a-Si:H imaging arrays. *MRS Proc* 1993;297:945–950.
29. Lee DLY, Cheung LK, Jeromin LS. New digital detector for projection radiography. In: Van Metter RL, Beutel J, eds. *Proceedings of SPIE: medical imaging 1995—physics of medical imaging*. Vol 2432. Bellingham, Wash: SPIE—The International Society for Optical Engineering, 1995; 237–249.
30. Zhao W, Rowlands JA. Large-area solid state detector for radiology using amorphous selenium. In: Shaw R, ed. *Proceedings of SPIE: medical imaging 1992—instrumentation*. Vol 1651. Bellingham, Wash: SPIE—The International Society for Optical Engineering, 1992; 134–143.
31. Zhao W, Rowlands JA. X-ray imaging using amorphous selenium: feasibility of a flat panel self-scanned detector for digital radiology. *Med Phys* 1995;22(10):1595–1604.
32. Zhao W, Rowlands JA. Digital radiology using active matrix readout of amorphous selenium: theoretical analysis of detective quantum efficiency. *Med Phys* 1997;24(12):1819–1833.
33. Busse F, Ruetten W, Sandkamp B, Alving PL, Bastiaens RJM, Ducourant T. Design and performance of a high-quality cardiac flat detector. In: Antonuk LE, Yaffe MJ, eds. *Proceedings of SPIE: medical imaging 2002—physics of medical imaging*. Vol 4682. Bellingham, Wash: SPIE—The International Society for Optical Engineering, 2002; 819–827.
34. Schiebel UW, Conrads N, Jung N, et al. Fluoroscopic x-ray imaging with amorphous silicon thin-film arrays. In: Shaw R, ed. *Proceedings of SPIE: medical imaging 1994—physics of medical imaging*. Vol 2163. Bellingham, Wash: SPIE—The International Society for Optical Engineering, 1994; 129–140.
35. Parker DL. Optimal short scan convolution reconstruction for fanbeam CT. *Med Phys* 1982;9(2):254–257.
36. Leschka SC, Babic D, El Shikh S, Wossmann C, Schumacher M, Taschner CA. C-arm cone beam computed tomography needle path overlay for image-guided procedures of the spine and pelvis. *Neuroradiology* 2012;54(3):215–223.
37. Kothary N, Abdelmaksoud MH, Tognolini A, et al. Imaging guidance with C-arm CT: prospective evaluation of its impact on patient radiation exposure during transhepatic arterial chemoembolization. *J Vasc Interv Radiol* 2011;22(11):1535–1543.
38. Lin M, Loffroy R, Noordhoek N, et al. Evaluating tumors in transcatheter arterial chemoembolization (TACE) using dual-phase cone-beam CT. *Minim Invasive Ther Allied Technol* 2011;20(5):276–281.
39. Loffroy R, Lin M, Yenokyan G, et al. Intra-procedural C-arm dual-phase cone-beam CT: can it be used to predict short-term response to TACE with drug-eluting beads in patients with hepatocellular carcinoma? *Radiology* 2013;266(2):636–648.
40. Schulz B, Heidenreich R, Heidenreich M, et al. Radiation exposure to operating staff during rotational flat-panel angiography and C-arm cone beam computed tomography (CT) applications. *Eur J Radiol* 2012;81(12):4138–4142.
41. Suzuki S, Yamaguchi I, Kidouchi T, Yamamoto A, Masumoto T, Ozaki Y. Evaluation of effective dose during abdominal three-dimensional imaging for three flat-panel-detector angiography systems. *Cardiovasc Intervent Radiol* 2011;34(2):376–382.
42. Paul J, Jacobi V, Farhang M, Bazrafshan B, Vogl TJ, Mbalisike EC. Radiation dose and image quality of X-ray volume imaging systems: cone-beam computed tomography, digital subtraction angiography and digital fluoroscopy. *Eur Radiol* 2013;23(6):1582–1593.
43. Bai M, Liu B, Mu H, Liu X, Jiang Y. The comparison of radiation dose between C-arm flat-detector CT (DynaCT) and multi-slice CT (MSCT): a phantom study. *Eur J Radiol* 2012;81(11):3577–3580.
44. Kwok YM, Irani FG, Tay KH, Yang CC, Padre CG, Tan BS. Effective dose estimates for cone beam computed tomography in interventional radiology. *Eur Radiol* 2013; 23(11):3197–3204.
45. Tyan YS, Li YY, Ku MC, Huang HH, Chen TR. The effective dose assessment of C-arm CT in hepatic arterial embolisation therapy. *Br J Radiol* 2013;86(1024):20120551.
46. Ho LM, Yoshizumi TT, Hurwitz LM, et al. Dual energy versus single energy MDCT: measurement of radiation dose using adult abdominal imaging protocols. *Acad Radiol* 2009; 16(11):1400–1407.
47. Miller DL, Balter S, Wagner LK, et al. Quality improvement guidelines for recording patient radiation dose in the medical record. *J Vasc Interv Radiol* 2009;20(7 Suppl):S200–S207.
48. Gonzalez-Guindalini FD, Ferreira Botelho MP, Töre HG, Ahn RW, Gordon LI, Yaghmai V. MDCT of chest, abdomen, and pelvis using attenuation-based automated tube voltage selection in combination with iterative reconstruction: an inpatient study of radiation dose and image quality. *AJR Am J Roentgenol* 2013;201(5):1075–1082.
49. Miyayama S, Yamashiro M, Hattori Y, et al. Efficacy of cone-beam computed tomography during transcatheter arterial chemoembolization for hepatocellular carcinoma. *Jpn J Radiol* 2011;29(6):371–377.
50. Wallace MJ. C-arm computed tomography for guiding hepatic vascular interventions. *Tech Vasc Interv Radiol* 2007;10(1):79–86.
51. Yu L, Vrieze TJ, Bruesewitz MR, et al. Dose and image quality evaluation of a dedicated cone-beam CT system for high-contrast neurologic applications. *AJR Am J Roentgenol* 2010;194(2):W193–W201.
52. Schäfer D, Lin M, Rao PP, et al. Improved C-arm cone-beam CT imaging in the rabbit VX-2 liver tumor model by faster image acquisition and compensating for breathing motion: first results [abstr]. In: *Radiological Society of North America Scientific Assembly and Annual Meeting Program*. Oak

- Brook, Ill: Radiological Society of North America, 2011; 412.
53. Schäfer D, Ahrens M, Eshuis P, Grass M. Low kV rotational 3D x-ray imaging for improved CNR of iodine contrast agent. In: Pelc NJ, Nishikawa RM, Whiting BR, eds. *Proceedings of SPIE: medical imaging 2012—physics of medical imaging*. Vol 8313. Bellingham, Wash: SPIE—The International Society for Optical Engineering, 2012; 83132V.
  54. Schäfer D, Borgert J, Rasche V, Grass M. Motion-compensated and gated cone beam filtered back-projection for 3-D rotational X-ray angiography. *IEEE Trans Med Imaging* 2006;25(7):898–906.
  55. Schäfer D, Lin M, Rao PP, et al. Breathing motion compensated reconstruction for C-arm cone beam CT imaging: initial experience based on animal data. In: Pelc NJ, Nishikawa RM, Whiting BR, eds. *Proceedings of SPIE: medical imaging 2012—physics of medical imaging*. Vol 8313. Bellingham, Wash: SPIE—The International Society for Optical Engineering, 2012; 83131D.
  56. Tacher V, Bhagat N, Rao PV, et al. Image quality improvements in C-Arm CT (CACT) for liver oncology applications: preliminary study in rabbits. *Minim Invasive Ther Allied Technol* 2013;22(5):297–303.
  57. Rao PP, Lin M, Bhagat N, et al. Improving C-arm cone beam CT: protocol optimization and reducing motion artifacts for preclinical imaging [abstr]. In: *Radiological Society of North America Scientific Assembly and Annual Meeting Program*. Oak Brook, Ill: Radiological Society of North America, 2011; 228.
  58. Deschamps F, Solomon SB, Thornton RH, et al. Computed analysis of three-dimensional cone-beam computed tomography angiography for determination of tumor-feeding vessels during chemoembolization of liver tumor: a pilot study. *Cardiovasc Intervent Radiol* 2010;33(6):1235–1242.
  59. Miyayama S, Yamashiro M, Hashimoto M, et al. Identification of small hepatocellular carcinoma and tumor-feeding branches with cone-beam CT guidance technology during transcatheter arterial chemoembolization. *J Vasc Interv Radiol* 2013;24(4):501–508.
  60. Tacher V, Lin M, Chao M, et al. Semiautomatic volumetric tumor segmentation for hepatocellular carcinoma: comparison between C-arm cone beam computed tomography and MRI. *Acad Radiol* 2013;20(4):446–452.
  61. Meyer BC, Frericks BB, Voges M, et al. Visualization of hypervascular liver lesions During TACE: comparison of angiographic C-arm CT and MDCT. *AJR Am J Roentgenol* 2008;190(4):W263–W269.
  62. Bouvier A, Ozenne V, Aubé C, et al. Transarterial chemoembolisation: effect of selectivity on tolerance, tumour response and survival. *Eur Radiol* 2011;21(8):1719–1726.
  63. Miyayama S, Matsui O, Yamashiro M, et al. Ultrasensitive transcatheter arterial chemoembolization with a 2-f tip microcatheter for small hepatocellular carcinomas: relationship between local tumor recurrence and visualization of the portal vein with iodized oil. *J Vasc Interv Radiol* 2007;18(3):365–376.
  64. Higashihara H, Osuga K, Onishi H, et al. Diagnostic accuracy of C-arm CT during selective transcatheter angiography for hepatocellular carcinoma: comparison with intravenous contrast-enhanced, biphasic, dynamic MDCT. *Eur Radiol* 2012;22(4):872–879.
  65. Iwazawa J, Ohue S, Hashimoto N, Abe H, Hamuro M, Mitani T. Detection of hepatocellular carcinoma: comparison of angiographic C-arm CT and MDCT. *AJR Am J Roentgenol* 2010;195(4):882–887.
  66. Loffroy R, Lin M, Rao P, et al. Comparing the detectability of hepatocellular carcinoma by C-arm dual-phase cone-beam computed tomography during hepatic arteriography with conventional contrast-enhanced magnetic resonance imaging. *Cardiovasc Intervent Radiol* 2012;35(1):97–104.
  67. Meyer BC, Frericks BB, Albrecht T, Wolf KJ, Wacker FK. Contrast-enhanced abdominal angiographic CT for intra-abdominal tumor embolization: a new tool for vessel and soft tissue visualization. *Cardiovasc Intervent Radiol* 2007;30(4):743–749.
  68. Miyayama S, Yamashiro M, Okuda M, et al. Usefulness of cone-beam computed tomography during ultrasensitive transcatheter arterial chemoembolization for small hepatocellular carcinomas that cannot be demonstrated on angiography. *Cardiovasc Intervent Radiol* 2009;32(2):255–264.
  69. Tognolini A, Louie JD, Hwang GL, Hofmann LV, Sze DY, Kothary N. Utility of C-arm CT in patients with hepatocellular carcinoma undergoing transhepatic arterial chemoembolization. *J Vasc Interv Radiol* 2010;21(3):339–347.
  70. Miyayama S, Matsui O, Yamashiro M, et al. Detection of hepatocellular carcinoma by CT during arterial portography using a cone-beam CT technology: comparison with conventional CTAP. *Abdom Imaging* 2009;34(4):502–506.
  71. Miyayama S, Yamashiro M, Okuda M, et al. Detection of corona enhancement of hypervascular hepatocellular carcinoma by C-arm dual-phase cone-beam CT during hepatic arteriography. *Cardiovasc Intervent Radiol* 2011;34(1):81–86.
  72. Ueda K, Matsui O, Kawamori Y, et al. Differentiation of hypervascular hepatic pseudolesions from hepatocellular carcinoma: value of single-level dynamic CT during hepatic arteriography. *J Comput Assist Tomogr* 1998;22(5):703–708.
  73. Koelblinger C, Schima W, Berger-Kulemann V, et al. C-arm CT during hepatic arteriography tumour-to-liver contrast: intraindividual comparison of three different contrast media application protocols. *Eur Radiol* 2013;23(4):938–942.
  74. Yumoto Y, Jinno K, Tokuyama K, et al. Hepatocellular carcinoma detected by iodized oil. *Radiology* 1985;154(1):19–24.
  75. Matsui O, Kadoya M, Suzuki M, et al. Work in progress: dynamic sequential computed tomography during arterial portography in the detection of hepatic neoplasms. *Radiology* 1983;146(3):721–727.
  76. Pellerin O, Lin M, Bhagat N, Ardon R, Mory B, Geschwind JF. Comparison of semi-automatic volumetric VX2 hepatic tumor segmentation from cone beam CT and multi-detector CT with histology in rabbit models. *Acad Radiol* 2013;20(1):115–121.
  77. Virmani S, Ryu RK, Sato KT, et al. Effect of C-arm angiographic CT on transcatheter arterial chemoembolization of liver tumors. *J Vasc Interv Radiol* 2007;18(10):1305–1309.
  78. Wang X, Shah RP, Maybody M, et al. Cystic artery localization with a three-dimensional angiography vessel tracking system compared with conventional two-dimensional angiography. *J Vasc Interv Radiol* 2011;22(10):1414–1419.
  79. Takayasu K, Moriyama N, Muramatsu Y, et al. Gallbladder infarction after hepatic artery embolization. *AJR Am J Roentgenol* 1985;144(1):135–138.
  80. Tacher V, Lin M, Bhagat N, et al. Dual-phase cone-beam computed tomography to see, reach, and treat hepatocellular carcinoma during drug-eluting beads transarterial chemo-embolization. *J Vis Exp* 2013;(82):50795.
  81. Tognolini A, Louie J, Hwang G, Hofmann L, Sze D, Kothary N. C-arm computed tomography for hepatic interventions: a practical guide. *J Vasc Interv Radiol* 2010;21(12):1817–1823.
  82. Kim HC, Chung JW, Lee W, Jae HJ, Park JH. Recognizing extrahepatic collateral vessels that supply hepatocellular carcinoma to avoid complications of transcatheter arterial chemoembolization. *RadioGraphics* 2005;25(Suppl 1):S25–S39.
  83. Kim HC, Chung JW, An S, et al. Left inferior phrenic artery feeding hepatocellular carcinoma: angiographic anatomy using C-arm CT.

- AJR Am J Roentgenol 2009;193(4):W288–W294.
84. Kim HC, Chung JW, Lee IJ, et al. Intercoastal artery supplying hepatocellular carcinoma: demonstration of a tumor feeder by C-arm CT and multidetector row CT. *Cardiovasc Intervent Radiol* 2011;34(1):87–91.
  85. Iwazawa J, Ohue S, Mitani T, et al. Identifying feeding arteries during TACE of hepatic tumors: comparison of C-arm CT and digital subtraction angiography. *AJR Am J Roentgenol* 2009;192(4):1057–1063.
  86. Riaz A, Miller FH, Kulik LM, et al. Imaging response in the primary index lesion and clinical outcomes following transarterial locoregional therapy for hepatocellular carcinoma. *JAMA* 2010;303(11):1062–1069.
  87. Gillmore R, Stuart S, Kirkwood A, et al. EASL and mRECIST responses are independent prognostic factors for survival in hepatocellular cancer patients treated with transarterial embolization. *J Hepatol* 2011;55(6):1309–1316.
  88. Shim JH, Lee HC, Kim SO, et al. Which response criteria best help predict survival of patients with hepatocellular carcinoma following chemoembolization? A validation study of old and new models. *Radiology* 2012;262(2):708–718.
  89. Therasse P, Arbutck SG, Eisenhauer EA, et al. New guidelines to evaluate the response to treatment in solid tumors. European Organization for Research and Treatment of Cancer, National Cancer Institute of the United States, National Cancer Institute of Canada. *J Natl Cancer Inst* 2000;92(3):205–216.
  90. Monsky WL, Kim I, Loh S, et al. Semi-automated segmentation for volumetric analysis of intratumoral ethiodol uptake and subsequent tumor necrosis after chemoembolization. *AJR Am J Roentgenol* 2010;195(5):1220–1230.
  91. Jeon UB, Lee JW, Choo KS, et al. Iodized oil uptake assessment with cone-beam CT in chemoembolization of small hepatocellular carcinomas. *World J Gastroenterol* 2009;15(46):5833–5837.
  92. Iwazawa J, Ohue S, Kitayama T, Sassa S, Mitani T. C-arm CT for assessing initial failure of iodized oil accumulation in chemoembolization of hepatocellular carcinoma. *AJR Am J Roentgenol* 2011;197(2):W337–W342.
  93. Mirpour S, Geschwind JH, Tacher V, et al. Lipiodol tumor uptake as an imaging biomarker: preclinical study. *J Vasc Interv Radiol* 2013;24(7):1080–1081.
  94. Sun JH, Wang LG, Bao HW, et al. Usefulness of C-arm angiographic computed tomography for detecting iodized oil retention during transcatheter arterial chemoembolization of hepatocellular carcinoma. *J Int Med Res* 2010;38(4):1259–1265.
  95. Chen R, Geschwind JF, Wang Z, Tacher V, Lin M. Quantitative assessment of lipiodol deposition after chemoembolization: comparison between cone-beam CT and multidetector CT. *J Vasc Interv Radiol* 2013;24(12):1837–1844.
  96. Wang Z, Lin M, Lesage D, et al. Three-dimensional evaluation of lipiodol retention in HCC after chemoembolization: a quantitative comparison between CBCT and MDCT. *Acad Radiol* 2014;21(3):393–399.
  97. Lewandowski RJ, Geschwind JF, Liapi E, Salem R. Transcatheter intraarterial therapies: rationale and overview. *Radiology* 2011;259(3):641–657.
  98. Lencioni R, de Baere T, Burrel M, et al. Transcatheter treatment of hepatocellular carcinoma with Doxorubicin-loaded DC Bead (DEBDOX): technical recommendations. *Cardiovasc Intervent Radiol* 2012;35(5):980–985.
  99. Suk Oh J, Jong Chun H, Gil Choi B, Gyu Lee H. Transarterial chemoembolization with drug-eluting beads in hepatocellular carcinoma: usefulness of contrast saturation features on cone-beam computed tomography imaging for predicting short-term tumor response. *J Vasc Interv Radiol* 2013;24(4):483–489.